Theoretical study of dielectronic recombination between electrons and heliumlike carbon ions

Ya-Qiong Xu,[1] Yi-Zhi Qu,[1,2,3] Xiang-Hui Zhang,[2] and Jia-Ming Li[1,2]
[1]*Institute of Physics, P.O. Box 603, Chinese Academy of Sciences, Beijing 100080, China*
[2]*Center of Atomic and Molecular Sciences, Department of Physics, Tsinghua University, Beijing 100084, China*
[3]*Graduate School, University of Science and Technology of China, Beijing 100039, China*
(Received 17 December 1999; published 20 July 2000)

A revised simplified relativistic configuration-interaction method is used to study the dielectronic recombination processes of He-like carbon ions. Every resonance of type $1s2Lnl$ has been determined for $n=2,3$. The total integrated cross sections of the dielectronic recombination are in agreement with the experimental measurements within 10%. It is found that the strong resonance peak around 283 eV consists of three important doubly excited resonance states with the dominant contribution due to two $(1s2p\ ^1P)\ 3d\ ^2F_{5/2,7/2}$ states, in contrast to the previous assignment of $(1s2p\ ^1P)\ 3p\ ^2S_{1/2}$ as the dominant resonance state.

PACS number(s): 34.80.Kw, 34.80.Dp

I. INTRODUCTION

Dielectronic recombination (DR) is a resonant radiative recombination process. When a free electron collisionally excites an ion C^{4+}, it may lose enough energy to be captured into an unoccupied orbital nl, and one of the bound electrons of the ion C^{4+} is excited from the initial $1s$ orbital into the $2L$ orbital forming a doubly excited resonance state $1s2Lnl$. Subsequently, the doubly excited resonance state decays into states of C^{3+} through radiative transition processes. DR processes are fundamental recombination processes because of their importance in influencing the ionic balance in high-temperature plasmas and for understanding the dynamics of the solar corona [1]. Furthermore, their radiative emissions have significant effects on plasma cooling as well as the plasma diagnostic spectrum in fusion plasmas. Therefore they attract considerable interest from both experimental and theoretical researchers.

There are many theoretical methods by which to calculate the DR processes, such as distorted wave methods [2,3], close-coupling methods [4,5], relativistic close coupling using the Breit-Pauli *R*-matrix method [6], and single- and multiconfiguration methods [7–14]. In these calculations [7–10], it is generally tedious work to obtain all the accurate DR rate coefficients because they involve many doubly excited resonance states. Most calculations either neglect the high-lying doubly excited states or simply use the n^{-3} law to extrapolate for high-lying doubly excited states based on quantum defect theory (QDT) [8,15–17]. However, in the framework of QDT, we have developed a simplified relativistic configuration-interaction (SRCI) method to treat the high-lying doubly excited states by interpolations instead of extrapolations [11–14]. We have calculated the DR cross sections of H-like helium ions [12] and argon ions [13] and obtained good agreement with experimental results. Recent experiments on DR between electrons and He-like carbon ions have been performed by Mannervik *et al.* [18] with an energy resolution of 0.1 eV, which requires more accurate theoretical calculations. This present paper presents our theoretical study of DR processes between electrons and He-like carbon ions. To treat the electron correlations properly, it is important to include more configuration interactions, such as the orbital angular momentum correlations (i.e., l mixture). Thus, in this paper, we have developed a revised SRCI method including the orbital angular momentum correlations. Comparing the theoretical results calculated by the revised SRCI method (l mixture) with those calculated by the SRCI method (without l mixture), we find the orbital angular momentum correlations are important for detailed description of the peak positions and line shapes, even for the integrated cross sections. Both the integrated cross sections and the detailed line shapes are in good agreement with the experimental results [18] and also agree with the recent calculated results of Pradhan and Zhang [6]. Then we can give clear assignments of all the resonances for $1s2Lnl$ with $n=2,3$. For example, the resonance peak around 283 eV was identified as the only resonance state $(1s2p\ ^1P)3p\ ^2S$ in other theoretical work [18,19], while in our calculation we find this resonance peak consists of the three major states $(1s2p\ ^1P)3d\ ^2F_{5/2,7/2}$ and $(1s2p\ ^1P)3p\ ^2S_{1/2}$, and the integrated cross section of ^2F (~ 63) is larger than that of $^2S(\sim 7)$ (the units of the integrated cross section are 10^{-21} cm^2 eV throughout this paper, unless specified otherwise). The integrated cross section for these three states is 70.5, which is in fair agreement with the experimental result (~ 89) [18]. A more detailed analysis will be discussed in Sec. III. Because of its relativistic treatment, our revised SRCI method is applicable for arbitrary high-Z ions with much less computational effort and it can meet the needs of relevant applications.

II. THEORETICAL METHOD AND RESULTS

The DR process of C^{4+} is expressed as

$$e^- + C^{4+}(1s^2) \rightarrow C^{3+}(1s2Lnl)^{**} \rightarrow C^{3+}(1sN_kL_kn_kl_k)^* + h\nu, \qquad (1)$$

where the C^{4+} ion in the initial state i, with the major configuration $1s^2$, captures a free electron with a specific energy ϵ_i and forms the C^{3+} ion in the doubly excited resonance state j with the major configuration

$[(1s2L^{2S_c+1}L_c)nl^{2S_t+1}L_t]$ (L_c and S_c are the orbital angular momentum and spin quantum numbers for the C^{4+} ion and L_t and S_t are the total orbital angular momentum and spin quantum numbers for the C^{3+} ion). Under the isolated resonance approximation, the DR cross sections for any doubly excited resonance states can be expressed as

$$\sigma_{ij;k}=\frac{\pi^2\hbar^3}{m_e\epsilon_i}\frac{g_j}{2g_i}\frac{A^a_{ji}A^r_{jk}}{\Sigma_{k'}A^r_{jk'}+\Sigma_{i'}A^a_{ji'}}\delta(\epsilon-\epsilon_i), \tag{2}$$

where m_e is the mass of the electron. g_i and g_j are the statistical weights of the states i and j, respectively. A^a_{ji} is the Auger decay rate (inverse resonance capture process), which can be calculated by the Fermi golden rule. A^r_{jk} is the radiative rate from the upper state j to the lower state k. The summation i' is over all possible lower states of C^{4+}, and the summation k' is over all possible lower states of C^{3+}. The atomic wave function for the state j is expressed as

$$\Psi_j=\sum_d C_{jd}\phi(\Gamma_d). \tag{3}$$

Here $\phi(\Gamma_d)$ is the configuration wave function. Γ denotes the quantum numbers of the configuration $\Pi_i(n_i,\kappa_i)^{\omega_i}$ with a certain coupling scheme, where n_i,κ_i,ω_i are the principal quantum number, the combined quantum number of (l,j), and the occupation number, respectively. It is constructed as antisymmetrized product-type wave functions from central-field Dirac orbitals with the appropriate angular momentum coupling [20]. All relativistic single-electron wave functions (bound and continuum) are calculated based on the atomic self-consistent potential obtained from the ground-state configuration $(1s^22s\,^2S_{1/2})$ for C^{3+} [21,22]. In the SRCI method, the summation is over all configuration wave functions with the same principal quantum number n and the same orbital angular momentum quantum numbers (L,l). For example, for the doubly excited state $(1s2s\,^3S)3d\,^2D_{3/2}$, in our SRCI calculation, the summation in Eq. (3) includes three configuration wave functions, $(1s2s\,^3S_0)3d_{3/2}\,^2D_{3/2}$, $(1s2s\,^3S_1)3d_{3/2}\,^2D_{3/2}$, and $(1s2s\,^3S_1)3d_{5/2}\,^2D_{3/2}$. In the present revised SRCI method, the configuration wave functions $\phi(\Gamma_d)$ with the same n and different (L,l) are added into the summation (i.e., l mixture). The mixing coefficients C_{jd} for state j are obtained by diagonalizing the relevant Hamiltonian matrix [20].

We neglect the configuration interactions between bound states with different n and continuum states. Then we have

$$A^a_{ji}=\frac{2\pi}{\hbar}\left|\sum_d C_{jd}M^a_{ijd}\right|^2, \tag{4}$$

where the Auger decay matrix element M^a_{ijd} is defined as

$$M^a_{ijd}=\left\langle \phi(\Gamma_d)\left|\sum_{s<f}\frac{1}{r_{s,f}}\right|\Psi_{i\epsilon_i}\right\rangle. \tag{5}$$

Here $\Psi_{i\epsilon_i}$ consists of the C^{4+} ion state wave function and a single-electron wave function in the continuum.

Based on QDT, when (L,l) are fixed and n varies from bound to continuum states, all the doubly excited resonance states with the same total angular momentum J and coupling scheme will form a channel. In the channel, the energy-normalized matrix element can be defined as

$$\bar{M}^a_{ijd}=M^a_{ijd}(\nu_n^{3/2}/q); \tag{6}$$

here (ν_n^3/q^2) is the density of states, $\nu_n=n-\mu_n$, and μ_n is the corresponding quantum defect. This energy-normalized matrix element $\bar{M}^a_{ijd}$ varies smoothly with the electron orbital energy in the channel [11,12]. When the $\bar{M}^a_{ijd}$ of a few states (including one continuum state) in a channel have been calculated, the Auger decay matrix elements of infinitely many discrete states of that channel can be obtained by interpolation. On the other hand, the mixing coefficients C_{jd} in Eq. (4) are almost unchanged for states with large n within a channel [12]. We can use the mixing coefficients of a state with a certain high principal quantum number n to approximate those of states with higher principal quantum number. From Eq. (5), the Auger rates and capture rates (by detailed balance) of the infinitely many doubly excited resonance states can be conveniently obtained.

The doubly excited resonance state may autoionize with a rate A^a_{ji} by reemitting an Auger electron or decay radiatively into a lower-energy state k with a radiative rate A^r_{jk}, which is defined as

$$A^r_{jk}=\frac{4e^2\omega}{3\hbar c^3 g_j}\left|\sum_{d,d'} C_{jd}C_{kd'}M^r_{jk}\right|^2, \tag{7}$$

where ω is the photon energy and the radiative transition matrix element is defined as

$$M^r_{jk}=\langle\phi(\Gamma_d)|T^{(1)}|\phi'(\Gamma'_d)\rangle. \tag{8}$$

For a radiative process with a certain final state k, when (L,l) are fixed and n varies from bound to continuum states, all the doubly excited resonance states with the same J and coupling scheme will form a channel. In the channel, the energy-normalized radiative transition matrix element is defined as

$$\bar{M}^r_{jk}=M^r_{jk}(\nu_n^{3/2}/q). \tag{9}$$

This energy-normalized matrix element $\bar{M}^r_{jk}$ varies slowly with the electron orbital energy [12,23,24]. When the $\bar{M}^r_{jk}$ of a few states (including one continuum state) in a channel have been calculated as benchmark points, all the energy-normalized matrix elements $\bar{M}^r_{jk}$ of infinitely many discrete states in that channel can be obtained by interpolation [23,24]. From expression (7), we can obtain all the radiative rates in the channel. For a certain initial state, the energy-normalized transition matrix element may have nodes, at which the matrix element is equal to zero [25]. In this case,

the interpolation should be carried out for the energy-normalized transition matrix elements and not for the radiative rates (i.e., it is proportional to the square of the transition elements).

The resonance energy ϵ_i can be calculated under the frozen core approximation [26]. Specifically, we can calculate the energy difference ΔE_{ic} between the total energy E_i of the doubly excited state $1s2Lnl$ of C^{3+} and the total energy E_c of the excited state of C^{4+} (the corresponding threshold) by the revised SRCI method. On the other hand, the excitation energy ΔE_c of the excited states of C^{4+} can be obtained from either an experimental or another independent theoretical result. Then the resonance energy ϵ_i can be calculated as $\Delta E_c + \Delta E_{ic}$, with a certain accuracy. The doubly excited resonance states with different principal quantum number n, corresponding to the same threshold and coupling scheme form a channel. Based on a finite set of benchmark values of the quantum defect μ in the channel, which are calculated by the revised SRCI method, the quantum defects and the energies of the infinitely many doubly excited states in the channel can be obtained by interpolation according to the quantum defect theory.

In order to compare with the experimental results, the calculated cross section should be convoluted with a Gaussian distribution of an energy resolution Γ, which is the summation of the experimental width Γ_T and the natural width Γ_N,

$$\Gamma = \sqrt{\Gamma_T^2 + \Gamma_N^2}, \tag{10}$$

where

$$\Gamma_N = \hbar \left(\sum_{k'} A^r_{jk'} + \sum_{i'} A^a_{ji'} \right). \tag{11}$$

The convoluted cross section is

$$\sigma_t^{DR}(\epsilon) = \sum_j \frac{S_{ij}}{\sqrt{2\pi}\Gamma} \exp\left(- \frac{(\epsilon - \epsilon_j)^2}{2\Gamma^2} \right), \tag{12}$$

where

$$S_{ij} = \frac{\pi^2 \hbar^3}{m_e \epsilon_i} \frac{g_j}{2g_i} \frac{A^a_{ji} \Sigma_k A^r_{jk}}{\Sigma_{k'} A^r_{jk'} + \Sigma_{i'} A^a_{ji'}}. \tag{13}$$

We have calculated the DR processes of He-like carbon ions and compared the calculated results with the experimental results for the doubly excited states $1s2Lnl$ with $n = 2,3$, as shown in Table I, Fig. 1(a), and Fig. 2(a). Both the integrated cross section and the line shapes are in agreement with the experimental results. Every resonance has also been identified.

In Table I, we have compared our calculated energy positions and integrated cross sections of the major doubly excited states with other theoretical [18,19] and experimental results [18]. They agree with each other in general. For example, for the weak resonance peak around 227 eV assigned as the resonance state $1s2s^2\,{}^2S_{1/2}$, our calculated integrated cross section (~ 0.7) is in good agreement with the experimental result (~ 0.7). In our revised SRCI method, the wave function in Eq. (3) of the resonance state with the major configuration $1s2s^2\,{}^2S_{1/2}$ consists of two important configuration wave functions, $1s2s^2\,{}^2S_{1/2}$ and $1s2p^2\ {}^2S_{1/2}$, so this resonance state can radiatively decay into $1s^2 2p\ {}^2P_{1/2,3/2}$, with a nonzero radiative matrix element. As shown in Table II, the radiative transition rate for the resonance state $1s2s^2\,{}^2S_{1/2}$ is 3.0×10^{10} (the units of the transition rate are $\sec^{-1}$ throughout this paper, unless specified otherwise). Furthermore, the configuration interactions influence not only the transition matrix elements (i.e., the cross sections), but also the energy positions (i.e., the resonance energies). For instance, the resonance state with the major configuration $1s2p^2\,{}^2S_{1/2}$ can consist of two configurations, namely, $1s2p^2\,{}^2S_{1/2}$ and $1s2s^2\,{}^2S_{1/2}$. The configuration interactions can change the resonance energy position of the resonance state $1s2p^2\,{}^2S_{1/2}$. In addition, in our calculation, we have found some doubly excited states, which are very important in DR processes, that have been overlooked in other theoretical work [18,19]. For instance, the resonance peak around 242 eV was identified as $1s2p^2\,{}^2D$ in Ref. [18], but in our calculation this peak consists of three major doubly excited states, $1s2p^2\,{}^2D_{3/2,5/2}$ and $1s2p^2\,{}^2P_{3/2}$, because of our fully relativistic treatment (i.e., configuration interactions through the orbital-spin interactions, which can be regarded as the ''relativistic effect'' in Ref. [27]). The integrated cross section of these three states is 42.9, in agreement with the work of Bellantone and Hahn (~ 42) [19] and the experimental result (~ 37) [18]. The wave function in Eq. (3) of the resonance state with the major configuration $1s2p^2\,{}^2P_{3/2}$ consists of two important configuration wave functions, namely, 99% of $1s2p^2\,{}^2P_{3/2}$ and 0.36% of $1s2p^2\,{}^2D_{3/2}$. The resonance state can be formed from the initial state $1s^2$ by capturing a free $d_{3/2}$ electron, with nonzero capture matrix element. As shown in Table II, the Auger width for this resonance state is 0.2 (the units of Auger width are meV throughout this paper, unless specified otherwise). Similarly, the resonance peak ranging from 281.0 to 281.6 eV was previously identified as $(1s2p\ {}^3P)3d\ {}^2P$ and $(1s2p\ {}^1P)3p\ {}^2D$ [18,19], but in our calculation this peak may consist of five main doubly excited states, $(1s2p\ {}^3P)3d\ {}^2P_{1/2,3/2}$, $(1s2p\ {}^1P)3p\ {}^2D_{3/2,5/2}$, and $(1s2p\ {}^1P)3p\ {}^2P_{3/2}$. The integrated cross section of these five states is 72.3, which is in good agreement with the experimental results (~ 73). In addition, another strong resonance peak around 283 eV was identified as $(1s2p\ {}^1P)3p\ {}^2S$ in Refs. [18,19], but this calculated integrated cross section (~ 4) [19] is obviously much smaller than the experimental result (~ 89). In our calculation this resonance peak may consist of three major doubly excited states, $(1s2p\ {}^1P)3d\ {}^2F_{5/2,7/2}$ and $(1s2p\ {}^1P)3p\ {}^2S_{1/2}$. The integrated cross section (~ 63) of ${}^2F$ is much larger than that (~ 7) of ${}^2S$. Our calculated integrated cross section of the three overlap states is 70.5, which is in fair agreement with the experimental result (~ 89) [18]. For more detailed analysis, we have found that the resonance states $(1s2p\ {}^1P)3d\ {}^2F_{5/2,7/2}$ have a strong radiative transition rate

TABLE I. Excitation energies relative to the ionization limit ($1s^2\,{}^1S$) in eV and integrated cross sections for major doubly excited states of C^{3+}.

State	Energy (eV)			Integrated cross section (10^{-21} cm^2 eV)			
	Theory		Experiment	Theory			Experiment
	Present	Ref. [18]	Ref. [18]	Present		Ref. [19]	Ref. [18]
$1s2s^2\,{}^2S_{1/2}$	226.764	227.13	227.10(9)	0.65			0.7(0.2)
$1s(2s2p\,{}^3P)^2P_{1/2}$	235.114	235.495	235.49(1)	10.77	32.25	39	39.3(6)
$1s(2s2p\,{}^3P)^2P_{3/2}$	235.13			21.58			
$1s(2s2p\,{}^1P)^2P_{1/2}$	239.427	238.96	238.99(2)	1.76	5.21	13.2	4.9(3)
$1s(2s2p\,{}^1P)^2P_{3/2}$	239.424			3.45			
$1s2p^2\,{}^2D_{3/2}$	242.043	242.029	242.05(1)	12.79	31.86[a]	42.2	37.2(6)[a]
$1s2p^2\,{}^2D_{5/2}$	242.032			19.07			
$1s2p^2\,{}^2P_{3/2}$	242.244	243.269		11[a]			
$1s2p^2\,{}^2S_{1/2}$	248.096	248.16	248.18(2)	5.7		8.4	5.9(3)
$(1s2s\,{}^3S)3s\,{}^2S_{1/2}$	270.655			0.29			
$(1s2s\,{}^3S)3p\,{}^2P_{1/2}$	271.705	271.896	271.87(2)	1.97	5.91	7.7	5.7(3)
$(1s2s\,{}^3S)3p\,{}^2P_{3/2}$	271.703			3.94			
$(1s2s\,{}^3S)3d\,{}^2D_{3/2}$	274.309	274.242	274.39(4)	1.18	2.95		2.5(3)
$(1s2s\,{}^3S)3d\,{}^2D_{5/2}$	274.309			1.77			
$(1s2s\,{}^1S)3s\,{}^2S_{1/2}$	274.72			1.37			
$(1s2s\,{}^1S)3p\,{}^2P_{1/2}$	276.518	276.526	276.57(2)	1.37	4.10	2.5	5.1(3)
$(1s2s\,{}^1S)3p\,{}^2P_{3/2}$	276.521			2.73			
$(1s2p\,{}^3P)3s\,{}^2P_{1/2}$	277.992	277.877	277.81(3)	1.99	5.85	31.3	6.0(3)
$(1s2p\,{}^3P)3s\,{}^2P_{3/2}$	278.017			3.86			
$(1s2s\,{}^1S)3d\,{}^2D_{3/2}$	278.729	278.684	278.60(4)	9.49	23.52[b]		16.2(6)[b]
$(1s2s\,{}^1S)3d\,{}^2D_{5/2}$	278.748			14.03			
$1s2p\,{}^3P)3p^2D_{3/2}$	279.235	279.063	279.10(4)	2.81	7.13[b]	11.3	16.2(7)[b]
$(1s2p\,{}^3P)3p^2D_{5/2}$	279.238			4.32			
$(1s2p\,{}^1P)3s\,{}^2P_{1/2}$	279.845	279.688	279.68(5)	9.11	27.34	11.2	27.1(7)
$(1s2p\,{}^1P)3s\,{}^2P_{3/2}$	279.839			18.23			
$(1s2p\,{}^3P)3d^2F_{5/2}$	280.065			1.29			
$(1s2p\,{}^3P)3d^2F_{7/2}$	280.087			1.63			
$(1s2p\,{}^3P)3p\,{}^2S_{1/2}$	280.353	280.066	280.14(7)	4.41		2.7	9.5(6)
$(1s2p\,{}^3P)3d^2P_{1/2}$	281.049	280.958	281.05(4)	0.78	2.34[c]	7.8	12.8(6)[c]
$(1s2p\,{}^3P)3d^2P_{3/2}$	281.039			1.56			
$(1s2p\,{}^1P)3p^2D_{3/2}$	281.572	281.563	281.59(1)	20.97	48.61[c]	21.8	60.0(9)[c]
$(1s2p\,{}^1P)3p^2D_{5/2}$	281.569			27.64			
$(1s2p\,{}^1P)3p^2P_{3/2}$	281.577			21.37[c]			
$(1s2p\,{}^1P3d^2F_{5/2}$	283.348			27.12	63.34[d]		
$(1s2p\,{}^1P)3d^2F_{7/2}$	283.337			36.22			
$(1s2p\,{}^1P)3p\,{}^2S_{1/2}$	283.367	282.614	282.69(1)	7.10[d]		4.3	89.0(10)[d]
$(1s2p\,{}^1P)3d^2P_{1/2}$	284.047	284.024	284.10(1)	2.40	7.15	1.3	15.0(4)
$(1s2p\,{}^1P)3d^2P_{3/2}$	284.052			4.75			

[a]The sum of the integrated cross sections for the resonance states $1s2p^2\,{}^2D_{3/2}$ and $1s2p^2\,2^D_{5/2}$ is 31.86; because the experimental resolution is limited, the experimental result 37.2(2) should correspond to the total result 42.86 for the three states $D_{3/2}$,$D_{5/2}$, and $P_{3/2}$.

[b]The total integrated cross section for the resonance states $(1s2s\,{}^1S)3d\,{}^2D_{3/2,5/2}$ and $(1s2p\,{}^3P)3p\,{}^2D_{3/2,5/2}$ is 30.65, which corresponds to the experimental result 32.4(13), the sum of 16.2(6) and 16.2(7).

[c]The total integrated cross section for the resonance states $(1s2p\,{}^3P)3d\,{}^2P_{1/2,3/2}$,$(1s2p\,{}^1P)3p\,{}^2D_{3/2,5/2}$, and $(1s2p\,{}^1P)3p\,{}^2P_{3/2}$ is 72.32, which corresponds to the experimental result 72.8(15), the sum of 12.8(6) and 60.0(9).

[d]The total integrated cross section for $(1s2p\,{}^1P)3d\,{}^2F_{5/2,7/2}$ and $(1s2p\,{}^1P)3p\,{}^2S_{1/2}$ is 70.5, which corresponds to the experimental result 89.0(10).

(6.0×10^{10}) and nonzero Auger width (2.6). This is why these resonance states have significant contributions to the integrated cross section. In Table II our calculated Auger widths and radiative transition rates for the $1s2L2l$ and $1s2L3l$ states of C^{4+} are, in general, consistent with those calculated by the saddle-point technique [18], except for the resonance states $1s2p^2\,{}^2P_{3/2}$,$(1s2p\,{}^3P)3d\,{}^2F_{5/2,7/2}$, and $(1s2p\,{}^1P)3d\,{}^2F_{5/2,7/2}$, which are discussed above.

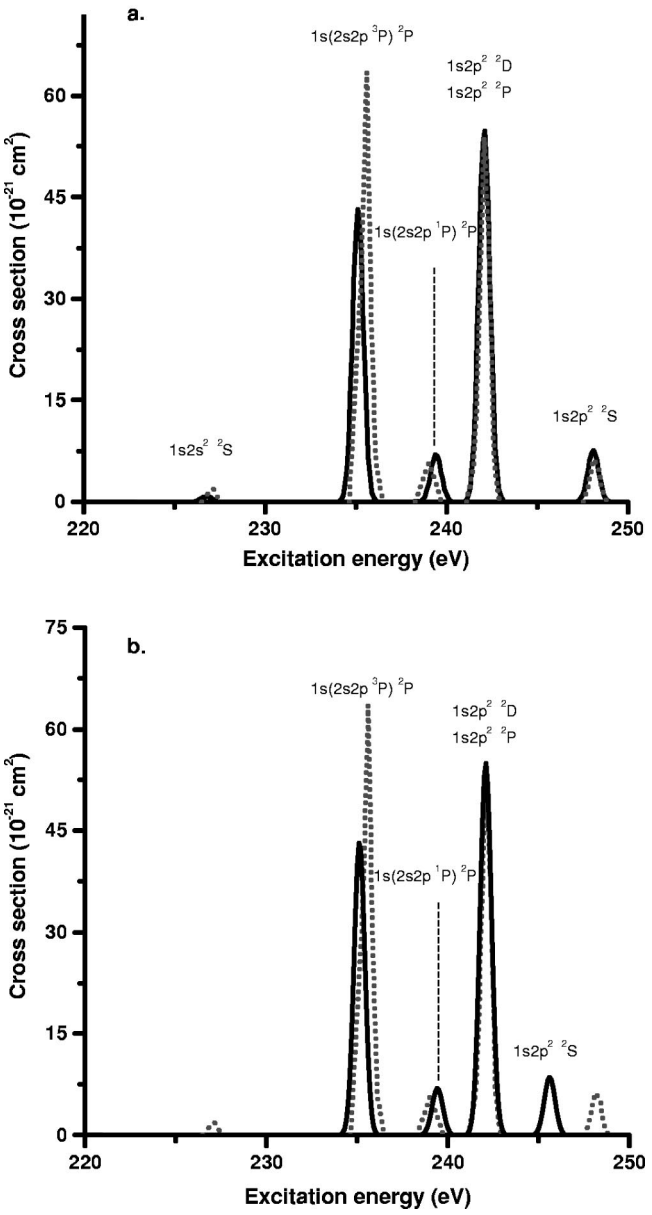

FIG. 1. Comparison of our calculated DR cross sections of He-like carbon for the $2L2l$ resonances (full line) with the experimental spectrum [18] (dotted line). (a) The theoretical cross section calculated by the revised SRCI method. (b) The theoretical cross section calculated by the SRCI method.

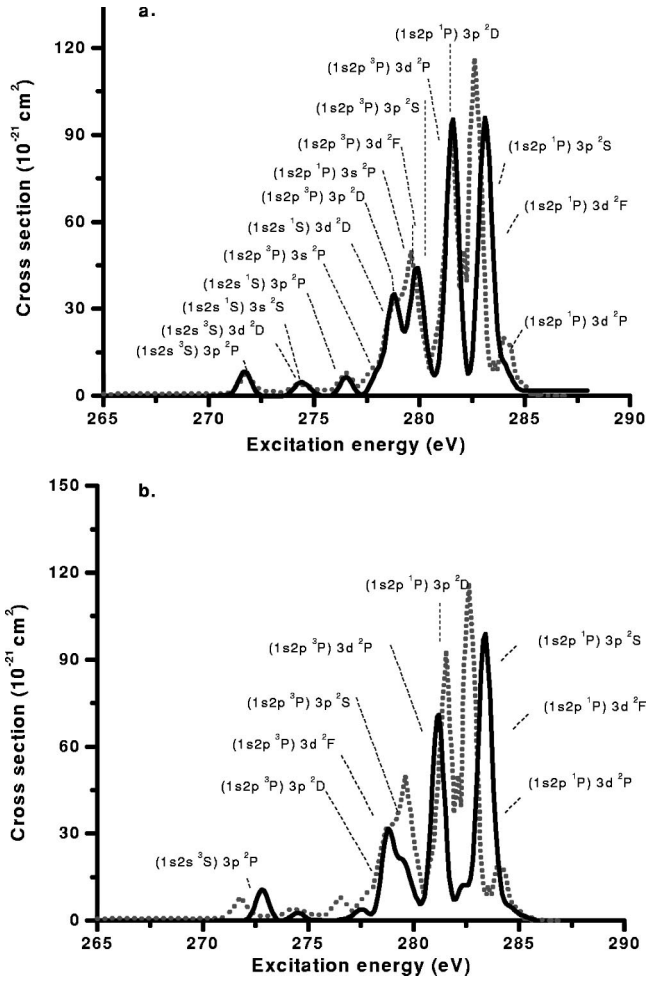

FIG. 2. Comparison of our calculated DR cross sections of He-like carbon for the $2L3l$ resonances (full line) with the experimental spectrum [18] (dotted line). (a) The theoretical cross section calculated by the revised SRCI method. (b) The theoretical cross section calculated by the SRCI method.

III. DISCUSSION

In the present work, we have developed a revised SRCI method (with l mixture) to calculate the DR cross section for C^{4+}. Not only the integrated cross sections but also the peak positions as well as the detailed line shapes are in agreement with the experimental measurements, as shown in Table I, Fig. 1(a), and Fig. 2(a). In order to elucidate the importance of the configuration interactions with the orbital angular momentum correlations, we compare the results calculated by the revised SRCI method with the results by the SRCI method (without l mixture) as shown in Fig. 1(b) and Fig. 2(b).

In Fig. 1(b), the results calculated by the SRCI method do not have any resonance peak around 227 eV owing to the resonance state $1s2s^2\,^2S_{1/2}$. In addition, there is a significant difference of the resonance energy for the resonance state $1s2p^2\,^2S_{1/2}$, i.e., the calculated energy position is lower than the experimental result by about 3 eV. In Fig 1(a), however, in our revised SRCI method, not only does the resonance peak owing to the resonance state $1s2s^2\,^2S_{1/2}$ appear with the integrated cross section 0.7 in good agreement with the experimental result ($\sim$0.7), but also the calculated resonance energy and the profile of the resonance state $1s2p^2\,^2S_{1/2}$ are in good agreement with the experimental results (for more detailed explanations, see Sec. II). In addition, the total integrated cross section for $n=2$ calculated by the revised SRCI method is 83, which is in agreement with the experimental result ($\sim$89) and better than the result of the SRCI method ($\sim$78).

As shown in Fig 2(b), the energy positions of $(1s2s\,^3S)3p\,^2P$,$(1s2s\,^1S)3p\,^2P$,$(1s2p\,^3P)3d\,^2P$, and $(1s2p\,^1P)3p\,^2S$ deviate greatly from the experimental results. For the two resonance profiles $(1s2s\,^3S)3p\,^2P$

TABLE II. Auger width and radiative transition rates for $1s2L2l$ and $1s2L3l$ states of C^{4+}. Γ is the Auger width in meV. The radiative transition rates W are in sec^{-1}. The number in brackets denotes the power of 10 by which the preceding term is to be multiplied.

State	$W(1s^2 2p)$		$W(1s2s2p)$		$W(1s^2 3p)$		W_R		Γ (meV)	
	Present	Ref. [18]	Present		Present	Ref. [18]	Present	Ref. [18]	Present	Ref. [18]
$1s2s^2\ ^2S_{1/2}$	2.963(10)	3.678(10)				5.904(8)	2.96(10)	3.73(10)	65.66	68.02
$1s2p^2\ ^2S_{1/2}$	2.941(11)	3.074(11)				1.195(9)	2.95(11)	3.09(11)	6.308	7.857
$1s2p^2\ ^2P_{3/2}$	0.934(12)	1.096(12)				5.234(9)	0.93(12)	1.10(12)	0.231	
$1s2p^2\ ^2D_{3/2}$	3.137(11)	3.489(11)				2.791(9)	3.14(11)	3.51(11)	65.08	51.23
$1s2p^2\ ^2D_{5/2}$	3.117(11)									
$(1s2s\ ^3S)3s\ ^2S_{1/2}$	1.080(10)	5.312(9)			7.318(7)	2.399(8)	1.59(10)	5.55(9)	18.48	17.62
$(1s2s\ ^3S)3d\ ^2D_{3/2}$	7.362(9)	1.507(10)	1.616(10)		1.309(9)	2.678(8)	3.35(10)	1.53(10)	1.01	2.358
$(1s2s\ ^3S)3d\ ^2D_{5/2}$	6.941(9)		1.945(10)		1.270(9)		3.34(10)		1.01	
$(1s2s\ ^1S)3s\ ^2S_{1/2}$	3.334(9)	1.289(10)			6.320(10)	6.630(10)	7.65(10)	7.92(10)	9.62	9.66
$(1s2s\ ^1S)3d\ ^2D_{3/2}$	1.122(11)	7.403(10)			1.473(11)	1.171(11)	2.86(11)	1.91(11)	2.73	0.633
$(1s2s\ ^1S)3d\ ^2D_{5/2}$	1.089(11)				1.464(11)		2.82(11)		2.60	
$(1s2p\ ^3P)3p\ ^2D_{3/2}$	6.345(10)	8.865(10)			4.903(9)	2.292(9)	7.98(10)	9.09(10)	8.31	8.968
$(1s2p\ ^3P)3p\ ^2D_{5/2}$	6.638(10)				4.422(9)		8.17(10)		8.59	
$(1s2p\ ^3P)3p\ ^2S_{1/2}$	1.776(11)	1.798(11)			1.746(11)	6.098(10)	3.55(11)	2.41(11)	0.55	3.065
$(1s2p\ ^1P)3p\ ^2D_{3/2}$	4.789(10)	6.995(10)			5.691(11)	6.689(11)	6.25(11)	7.39(11)	8.45	9.562
$(1s2p\ ^1P)3p\ ^2D_{5/2}$	8.444(9)				5.186(11)		5.36(11)		15.25	
$(1s2p\ ^1P)3p\ ^2S_{1/2}$	2.891(8)	4.098(10)			4.383(11)	6.336(11)	4.49(11)	6.75(11)	2.84	5.515
$(1s2p\ ^1P)3p\ ^2P_{3/2}$	5.623(10)				5.805(11)		6.45(11)		6.96	
$1s(2s2p\ ^3P)^2P_{1/2}$	5.495(11)	6.700(11)		1.813(9)		9.243(7)	5.50(11)	6.72(11)	2.45	3.88
$1s(2s2p\ ^3P)^2P_{3/2}$	5.514(11)						5.51(11)		2.33	
$1s(2s2p\ ^1P)^2P_{1/2}$	8.450(10)	7.278(10)		3.865(8)		9.842(8)	8.54(10)	7.41(10)	44.27	39.91
$1s(2s2p\ ^1P)^2P_{3/2}$	8.261(10)						8.35(10)		44.17	
$(1s2s\ ^3S)3p\ ^2P_{1/2}$	1.066(11)	1.244(11)	9.536(9)	5.116(9)		8.853(7)	1.27(11)	1.30(11)	0.47	0.55
$(1s2s\ ^3S)3p\ ^2P_{3/2}$	1.067(11)		9.735(9)				1.28(11)		0.47	
$(1s2s\ ^1S)3p\ ^2P_{1/2}$	8.118(10)	5.58(10)	2.419(10)	3.985(10)	1.514(10)	2.336(10)	1.24(11)	1.19(11)	0.13	0.095
$(1s2s\ ^1S)3p\ ^2P_{3/2}$	8.107(10)		2.259(10)		1.150(10)		1.25(11)		0.13	
$(1s2p\ ^3P)3s\ ^2P_{1/2}$	7.094(8)	1.487(9)	1.033(11)	6.193(10)	5.325(8)	1.513(9)	1.12(11)	6.49(10)	14.39	13.89
$(1s2p\ ^3P)3s\ ^2P_{3/2}$	7.022(8)		1.000(11)		5.682(8)		1.09(11)		14.39	
$(1s2p\ ^1P)3s\ ^2P_{1/2}$	8.390(7)	2.037(10)	5.116(11)	6.526(11)	2.890(10)	3.849(10)	5.53(11)	7.12(11)	4.88	1.46
$(1s2p\ ^1P)3s\ ^2P_{3/2}$	8.708(7)		5.125(11)		2.919(10)		5.54(11)		4.78	
$(1s2p\ ^3P)3d\ ^2P_{1/2}$	6.494(9)	1.116(8)	1.608(10)	6.586(10)		5.511(9)	6.60(10)	7.15(10)	0.09	0.176
$(1s2p\ ^3P)3d\ ^2P_{3/2}$	6.562(9)		1.703(10)		2.149(10)		6.74(10)		0.09	
$(1s2p\ ^1P)3d\ ^2P_{1/2}$	1.188(9)	5.790(9)	1.011(10)	1.018(10)	6.193(11)	7.751(11)	6.60(11)	7.91(11)	0.11	0.201
$(1s2p\ ^1P)3d\ ^2P_{3/2}$	1.174(9)		1.005(10)		6.186(11)		6.60(11)		0.11	
$(1s2p\ ^3P)3d\ ^2F_{5/2}$					1.346(11)		1.52(11)		0.02	
$(1s2p\ ^3P)3d\ ^2F_{7/2}$					1.333(11)		1.50(11)		0.02	
$(1s2p\ ^1P)3d\ ^2F_{5/2}$					5.442(11)		5.95(11)		2.61	
$(1s2p\ ^1P)3d\ ^2F_{7/2}$					5.456(11)		5.96(11)		2.60	

(around 272 eV) and $(1s2s\ ^1S)3p\ ^2P$ (around 277 eV), the energy positions calculated by the SRCI method are higher than the experimental result by about 1 eV, while in Fig. 2(a), the calculated energy positions by the revised SRCI method are in good agreement with the experimental result. For the resonance profile $(1s2p\ ^3P)3d\ ^2P$ around 279 eV, the SRCI calculated line shapes differ greatly from the experimental result. In contrast to the experimental result, the red wing of the SRCI calculated resonance profile is sharper than its blue wing. However, in Fig 2(a), the profile near 279 eV calculated by the revised SRCI method agrees with the experiment result quite well. For the resonance profile around 281 eV, the SRCI calculated energy position is lower than the experimental result by about 0.5 eV and the peak cross section is also smaller than the experimental result. In Fig. 2(a), in the contrast, profile calculated by the revised SRCI method is in good agreement with the experimental results. For the strong resonance profile around 283 eV, the SRCI calculated resonance energy is higher than the experimental result by about 1 eV, while in Fig. 2(a), the energy difference ($\sim$0.6 eV) is smaller in the revised SRCI method (we will disscuss the details later). This strong peak was originally assiged as $(1s2p\ ^1P)3p\ ^2S$ in Refs. [18,19]. In our calculation this resonance profile consists of three major

doubly excited states, $(1s2p\,^1P)3d\,^2F_{5/2,7/2}$ and $(1s2p\,^1P)3p\,^2S_{1/2}$. The integrated cross section ($\sim$63) of ^2F is much larger than that ($\sim$7) of ^2S. Hence, this profile is dominated by $(1s2p\,^1P)3d\,^2F$. In addition, in the revised SRCI method, the calculated total integrated cross section for $n=3$ is 236, which agrees with the experimental result ($\sim$260) much better than does the SRCI result ($\sim$160). We have also compared our calculated results with other theoretical results [6] for $n=2,3$. They agree with each other in general. The calculated energy positions in the work of Pradhan and Zhang [6] are generally redshifted. For the strong resonance profile around 283 eV, the calculated resonance energy in [6] is lower than the experimental result [18] by about 1 eV, while our calculated resonance energy is higher than the experimental result by about 0.6 eV.

Let us return to discuss the energy difference between the calculated resonance energy position (around 283 eV) and the experimental result. In our revised SRCI calculation, the energy difference changes from 1 eV to 0.6 eV after we consider the orbital angular momentum correlations. This indicates that the orbital angular momentum correlations can influence the energy positions, but not enough. Thus, if one includes the configuration interactions with different principal quantum numbers n (i.e., the radial correlations), the energy positions are anticipated to be better. Configuration interactions with radial correlations would also be important for the doubly excited resonance states $(1s2Lnl)$ with high n. In addition, the present energy resolution of 0.1 eV is not enough to resolve the detailed structures of the resonance states $1s2Lnl$ with high n. Therefore, further theoretical studies are required with radial correlations and experimental studies with higher resolution.

In comparison with the work of Mannervik *et al.* [18], in which about 600–1000 terms are included, much less computation effort is required in our revised SRCI method. In addition, the revised SRCI method should be applicable for arbitrary high-Z ions because of its relativistic treatment, and it can also meet the needs of relevant applications.

ACKNOWLEDGMENTS

This work was partially supported by the Chinese Science and Technology Commission, the National High-Tech ICF Committee in China, Science and Technology Funds of CAEP, the Chinese Research Association for Atomic and Molecular Data, and the Chinese NSF.

[1] A. Burgess, Astrophys. J. **139**, 776 (1964).
[2] W. Eissner and M.J. Seaton, J. Phys. B **6**, 2187 (1972).
[3] D.R. Flower and J.M. Launay, J. Phys. B **5**, L207 (1972).
[4] H.E. Saraph and M.J. Seaton, Philos. Trans. R. Soc. London, Ser. A **271**, 1 (1971).
[5] J. Dubau, Ph.D. thesis, University of London, 1973.
[6] A.K. Pradban and H.L. Zhang, J. Phys. B **30**, L571 (1997).
[7] Y. Hahn, Phys. Rev. A **22**, 2896 (1980).
[8] D.J. McLaughlin and Y. Hahn, Phys. Rev. A **29**, 712 (1984).
[9] M.H. Chen, Phys. Rev. A **31**, 1449 (1985).
[10] H.P. Saha, Phys. Rev. A **49**, 894 (1994).
[11] Chen-zhong Dong, Yu Zou, Jian-Guo Wang, and Jia-Ming Li, Acta Phys. Sin. **44**, 1712 (1995).
[12] Jian-Guo Wang, Yi-Zhi Qu, and Jia-Ming Li, Phys. Rev. A **52**, 4274 (1996).
[13] Jian-Guo Wang, Yu Zou, Chen-Zhong Dong, and Jia-Ming Li, Chin. Phys. Lett. **12**, 530 (1995).
[14] Yi-Zhi Qu, Jian-Guo Wang, Jian-Kui Yuan, and Jia-Ming Li, Phys. Rev. A **57**, 1033 (1998).
[15] J. Nilson, J. Quant. Spectrosc. Radiat. Transf. **36**, 539 (1986).
[16] K.R. Karim and C.P. Bhalla, Phys. Rev. A **37**, 2599 (1988).
[17] K.R. Karim and C.P. Bhalla, Phys. Rev. A **43**, 615 (1992).
[18] S. Mannervik, S. Asp, L. Broström, D.R. DeWitt, J. Lidberg, R. Schuch, and K.T. Chung, Phys. Rev. A **55**, 1810 (1997).
[19] R. Bellantone and Y. Hahn, Phys. Rev. A **40**, 6913 (1989).
[20] Zhong-Xin Zhao and Jia-Ming Li, Acta Phys. Sin. **34**, 1469 (1985).
[21] Jia-Ming Li and Zhong-Xing Zhao, Acta Phys. Sin. **31**, 97 (1982).
[22] D.A. Liberman, D.T. Cromer, and J.T. Waber, Comput. Phys. Commun. **2**, 107 (1971).
[23] Lei Liu and Jia-Ming Li, Acta Phys. Sin. **42**, 1901 (1993).
[24] Jian-Guo Wang, Xiao-Ming Tong, and Jia-Ming Li, Acta Phys. Sin. **45**, 13 (1996); Yi-Zhi Qu, Jian-Guo Wang, and Jia-Ming Li, *ibid.* **46**, 249 (1997).
[25] X.L. Liang, and J.M. Li, Acta Phys. Sin. **34**, 1479 (1985); M.S. Wang, and R.H. Pratt, Phys. Rev. A **29**, 174 (1984); R.Y. Yin, and R.H. Pratt, *ibid.* **35**, 1154 (1987); X.M. Tong, L. Yang, and J.M. Li, Acta Phys. Sin. **38**, 407 (1989).
[26] C.M. Lee (Jia-Ming Li), Phys. Rev. A **10**, 584 (1974).
[27] S. Mannervik, D. DeWitt, L. Engström, J. Lidberg, E. Lindroth, R. Schuch, and W. Zonf, Phys. Rev. Lett. **81**, 313 (1998).